Spatiochromatic Receptive Field Properties Derived from Information-Theoretic Analyses of Cone Mosaic Responses to Natural Scenes

Eizaburo Doi
edoi@ucsd.edu
Institute for Neural Computation, University of California, San Diego, La Jolla, CA 92093, U.S.A., and Graduate School of Informatics, Kyoto University, Kyoto 606-8501, Japan

Toshio Inui
inui@cog.ist.i.kyoto-u.ac.jp
Graduate School of Informatics, Kyoto University, Kyoto 606-8501, Japan

Te-Won Lee
tewon@salk.edu
Institute for Neural Computation, University of California, San Diego, La Jolla, CA 92093, U.S.A., and Howard Hughes Medical Institute, Computational Neurobiology Laboratory, Salk Institute, La Jolla, CA 92037, U.S.A.

Thomas Wachtler
wachtler@biologie.uni-freiburg.de
Neurobiology and Biophysics, Institute of Biology III, Albert-Ludwigs-Universität, 79104 Freiburg, Germany

Terrence J. Sejnowski
terry@salk.edu
Institute for Neural Computation, University of California, San Diego, La Jolla, CA 92093, U.S.A., Howard Hughes Medical Institute, Computational Neurobiology Laboratory, Salk Institute, La Jolla, CA 92037, U.S.A., and Department of Biology, University of California, San Diego, La Jolla, CA 92093, U.S.A.

Neurons in the early stages of processing in the primate visual system efficiently encode natural scenes. In previous studies of the chromatic properties of natural images, the inputs were sampled on a regular array, with complete color information at every location. However, in the retina cone photoreceptors with different spectral sensitivities are arranged in a mosaic. We used an unsupervised neural network model to analyze the statistical structure of retinal cone mosaic responses to calibrated color natural images. The second-order statistical dependencies derived from the covariance matrix of the sensory signals were removed in the first stage

of processing. These decorrelating filters were similar to type I receptive fields in parvo- or konio-cellular LGN in both spatial and chromatic characteristics. In the subsequent stage, the decorrelated signals were linearly transformed to make the output as statistically independent as possible, using independent component analysis. The independent component filters showed luminance selectivity with simple-cell-like receptive fields, or had strong color selectivity with large, often double-opponent, receptive fields, both of which were found in the primary visual cortex (V1). These results show that the "form" and "color" channels of the early visual system can be derived from the statistics of sensory signals.

1 Introduction

New algorithms have recently been developed to test the hypothesis that sensory signals are transformed in the early stages of sensory processing to reduce the redundancy of the inputs (Barlow, 1961; Field, 1994). The spatial properties of ganglion cells in the retina and thalamocortical neurons in the lateral geniculate nucleus (LGN) are consistent with algorithms that use second-order statistics to decorrelate natural scenes (Atick, 1992; Atick & Redlich, 1993) and the localized and oriented simple cells in the primary visual cortex (V1) reduce higher-order statistics (Olshausen & Field, 1996; Bell & Sejnowski, 1997; van Hateren & van der Schaaf, 1998). These studies used gray-scale natural images. Natural color images have also been analyzed using RGB inputs (Tailor, Finkel, & Buchsbaum, 2000; Hoyer & Hyvarinen, 2000) and LMS inputs with the spectral sensitivities of the human L-, M-, and S-cone photoreceptors (Wachtler, Lee, & Sejnowski, 2001). In these studies, the images were sampled on a regular grid, with the color at each location represented as a vector of three elements. In the retina cone photoreceptors are arranged in a mosaic, with only one cone at each location. Thus, chromatic information in the retina is extracted by comparing the responses of different cone types at different locations, which requires spatial interaction. This is not the case for RGB or LMS color images, where the information for chromaticity is fully available at each pixel.

Here, we consider a model that incorporates the cone mosaic found in the trichromatic foveal region of primates. We adopt a hierarchical model that consists of a decorrelating stage corresponding to LGN and a subsequent independent component analysis (ICA) stage corresponding to V1 (Bell & Sejnowski, 1997). Applying biological and computational constraints at each level of processing allows a better comparison to the properties of neurons in the early visual system.

2 Methods

2.1 Cone Mosaic Responses. A small cone mosaic patch was used to model the trichromatic foveal region of the primate retina (see Figure 1). To

obtain estimates of the cone mosaic responses to natural scenes, we took natural images using a 3CCD camera and converted them into LMS images (see the appendix for details). By scanning the data set randomly with the cone mosaic, 507,904 samples were generated.

2.2 Model.

2.2.1 Computational Goal. We assume that the early stages of visual processing are linear,

$$\mathbf{u} = \mathbf{W}\mathbf{x}, \tag{2.1}$$

where $\mathbf{x} = (x_1, \ldots, x_n)^T$ are the input signals to the visual system (namely, the cone mosaic responses), $\mathbf{W} = [\mathbf{w_1}, \ldots, \mathbf{w_n}]^T$ is a square matrix consisting of receptive fields $\mathbf{w_i}$, and $\mathbf{u} = (u_1, \ldots, u_n)^T$ is the output, corresponding to the neural activities (Olshausen & Field, 1996; Bell & Sejnowski, 1997).

The computational goal of the system is assumed to reduce the redundancies or statistical dependencies among the output elements. This coding scheme is known as minimum entropy coding or factorial coding (Atick, 1992; Field, 1994) and can be implemented by ICA (Bell & Sejnowski, 1995; Lee, 1998; Girolami, 1999; Hyvarinen, Karhunen, & Oja, 2001).

A linear generative model for the input data $\mathbf{x}$ is given by

$$\mathbf{x} = \mathbf{A}\mathbf{s} = s_1\mathbf{a_1} + \cdots + s_n\mathbf{a_n}, \tag{2.2}$$

where $\mathbf{A} = [\mathbf{a_1}, \ldots, \mathbf{a_n}]$ is a set of basis functions and $s_1, \ldots, s_n$ are their coefficients, called sources or causes. Given sources $\mathbf{s}$ that are statistically independent of each other, equation 2.2 assumes that the input $\mathbf{x}$ is generated by a linear mixture of statistically independent causes $\mathbf{s}$. The goal of ICA is to find a matrix $\mathbf{W}$ that unmixes $\mathbf{x}$ so that $\mathbf{u} = \mathbf{s}$, namely, $\mathbf{W} = \mathbf{A}^{-1}$ (up to permutation and scaling).

The assumption of statistical independence among sources $\mathbf{s}$ and the general evidence of high redundancy in the sensory input $\mathbf{x}$ mean that the basis functions $\mathbf{a_i}$ introduce statistical dependency in the input. Equation 2.2 means that when a source s_i is activated (i.e., taking nonzero value), more than one sensor will concurrently have nonzero values according to the pattern of $\mathbf{a_i}$, which leads to statistical dependency in the sensory signals $\mathbf{x}$.

2.2.2 Hierarchical Implementation. We followed the approach of Bell and Sejnowski (1997) in decomposing the linear transformation $\mathbf{W}$ into decorrelation and ICA, $\mathbf{W_I}\mathbf{W_Z}$ (see Figure 2): the first operator $\mathbf{W_Z}$ decorrelates the input $\mathbf{x}$ such that the covariance matrix of its output $\mathbf{u_Z}$ satisfies

$$\langle \mathbf{u_Z}\mathbf{u_Z}^T \rangle = \langle (\mathbf{W_Z}\mathbf{x})(\mathbf{W_Z}\mathbf{x})^T \rangle = \mathbf{I}, \tag{2.3}$$
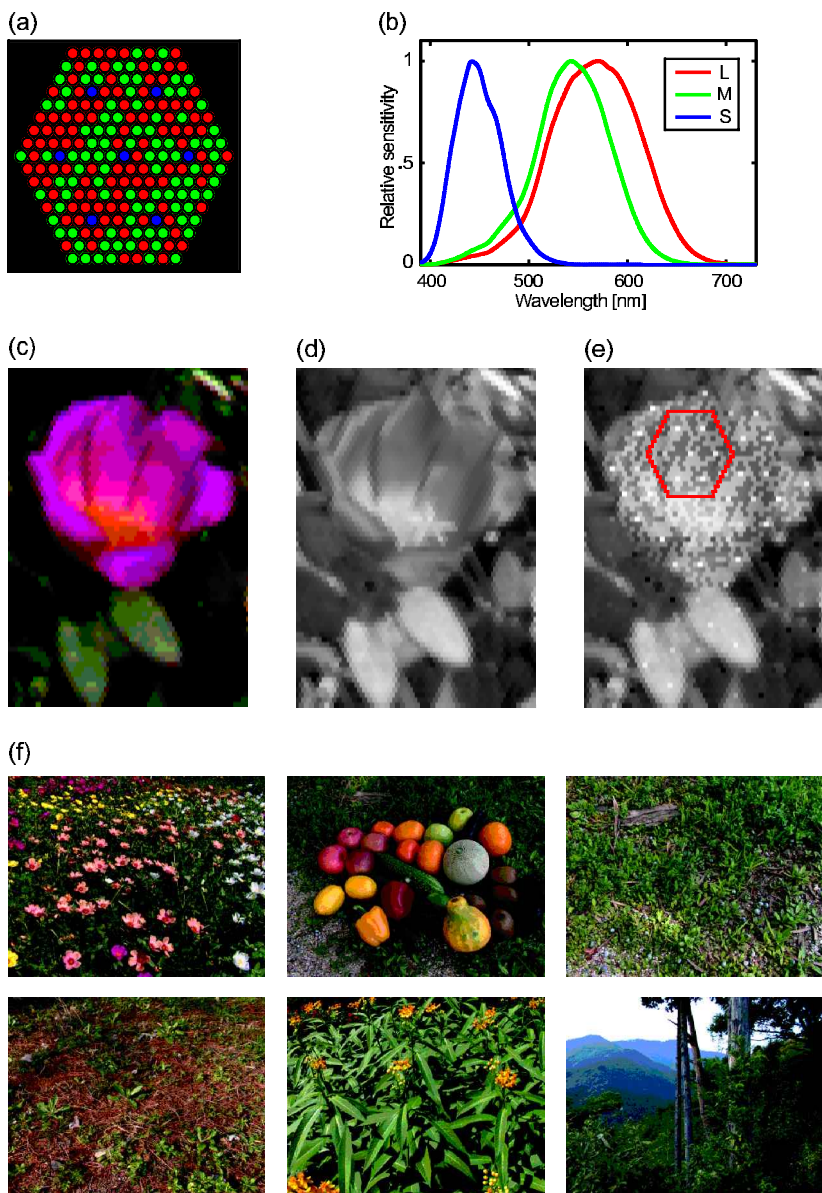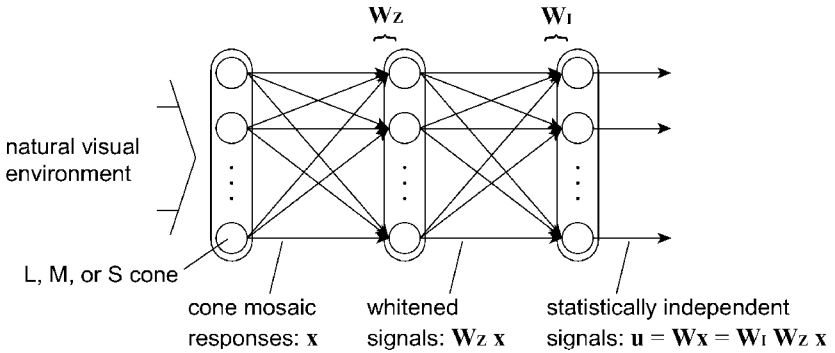
Figure 2: Three-stage model of the early visual system. This is three-layer feed-forward neural network. The first stage corresponds to the photoreceptor layer in the retina, as shown in Figure 1. The subsequent stages are assumed to reduce redundancy in the sensory input in a sequential manner.

where $\mathbf{I}$ is the identity matrix. This decorrelation normalizing the output variance is also known as the whitening transformation or zero-phase filters (Bell & Sejnowski, 1997). The second operator $\mathbf{W_I}$ makes the decorrelated signals $\mathbf{W_Z x}$ to be statistically as independent as possible (ICA for whitened data). This decomposition is justified as follows. First, the overlap of cone

---

Figure 1: *Facing page.* Properties of the input. (a) Cone mosaic model. This is based on the anatomical data from old world monkeys. It consists of 217 photoreceptors of L- (red), M- (green), and S-cone (blue). L- and M-cones are arranged randomly (Mollon & Bowmaker, 1992), whereas S-cones are arranged regularly (de Monasterio, McCrane, Newlander, & Schein, 1985; Szel, Diamantstein, & Rohlich, 1988). The cone ratio is L : M = 1 : 1 (Mollon & Bowmaker, 1992; Baylor et al., 1987), and S-cone occupies about 3% (de Monasterio et al., 1985; Mollon & Bowmaker, 1992). In this model L : M : S = 112 : 98 : 7. (b) Spectral sensitivities of cone photoreceptors. Here we used those of human cone photoreceptors (Stockman & Sharpe, 2000). (c–e) An example of cone mosaic output compared with RGB and gray-scale natural images. (c) RGB image. (d) Gray-scale image. M-cone responses are shown for reference. Larger responses correspond to brighter pixels. (e) Cone mosaic responses. The red hexagon shows the window of the cone mosaic shown in *a*; thus, the image inside is the response pattern of the cone mosaic. This image was prepared by concatenating several response patches of the same cone mosaic. The pixels are arranged in the hexagonal grid instead of a square grid to mimic the closely packed structure of the retinal cone mosaic as shown in *a*. They are generated by averaging four pixels of square-grid images with one pixel offset between each row. (f) Examples of natural images. Sixty-two natural images were used.

spectral sensitivities (especially between L- and M-cones) produces a strong correlation between elements of the input, as is the case of gray-scale natural images. This correlation could be removed as a first step toward a statistically independent representation. This operation restricts the solution of the next stage $\mathbf{W_I}$ to be in the orthogonal matrix manifold. Second, spatial properties of receptive fields of retinal ganglion cells and LGN cells have been suggested to be explained by decorrelation, using gray-scale data sets (Atick, 1992; Atick & Redlich, 1993; Bell & Sejnowski, 1997).

2.2.3 Learning Algorithms. $\mathbf{W_Z}$ is a whitening matrix that satisfies equation 2.3 with an additional degree of freedom in the choice of whitening matrix: if $\mathbf{W_Z}$ is a whitening matrix, $\mathbf{UW_Z}$ is also a whitening matrix for arbitrary orthogonal matrices $\mathbf{U}$. Here we assume that the whitening matrix is symmetric, $\mathbf{W_Z}^T = \mathbf{W_Z}$, which makes it unique. For gray-scale natural images, this whitening yields a set of zero-phase filters, which flatten the spatial-frequency ($1/f$) spectrum of shift-invariant data and show concentric center-surround receptive field organization (Atick, 1992; Atick & Redlich, 1993). Such a matrix can be derived by matrix square root of the inverse of the input covariance matrix (Golub & Loan, 1996; Bell & Sejnowski, 1997) or using a more biologically plausible learning algorithm (Atick & Redlich, 1993). Since both are equivalent, we used the former method for convenience.

The ICA algorithm we used can be derived using information maximization or maximum likelihood estimation (Bell & Sejnowski, 1995; Cardoso, 1997) with the natural gradient (Amari, Cichocki, & Yang, 1996),

$$\Delta\mathbf{W_I} \propto [\mathbf{I} - \varphi(\mathbf{u})\mathbf{u}]\mathbf{W_I}, \tag{2.4}$$

where $\varphi(\mathbf{u}) = -\frac{\partial \log p(\mathbf{u})}{\partial \mathbf{u}}$, $p(\mathbf{u}) = \Pi_i p(u_i)$ is the probability density of $\mathbf{u}$, and $\Delta\mathbf{W_I}$ is the change of weights computed iteratively until it converges to zero. Note that it requires a density model of $p(u_i)$. We use the extended infomax algorithm for ICA that assumes different $p(u_i)$'s for supergaussian and subgaussian density (Lee, Girolami, & Sejnowski, 1999). Thus, the results do not require the coefficients to have sparse distributions, unlike some previous methods (Olshausen & Field, 1996; Bell & Sejnowski, 1997).

3 Results

3.1 Decorrelating Stage. All units in the decorrelating stage showed concentric center-surround receptive field organization with the center region driven by a single cone (see Figure 3). Receptive fields of type I neurons of parvo- or konio-cellular LGN (pLGN/kLGN) of the macaque have these properties (Lennie & D'Zmura, 1988; in their review, as in this study, the properties of retinal ganglion cells were not distinguished from those of LGN cells). They can be further classified on the basis of the center-driving
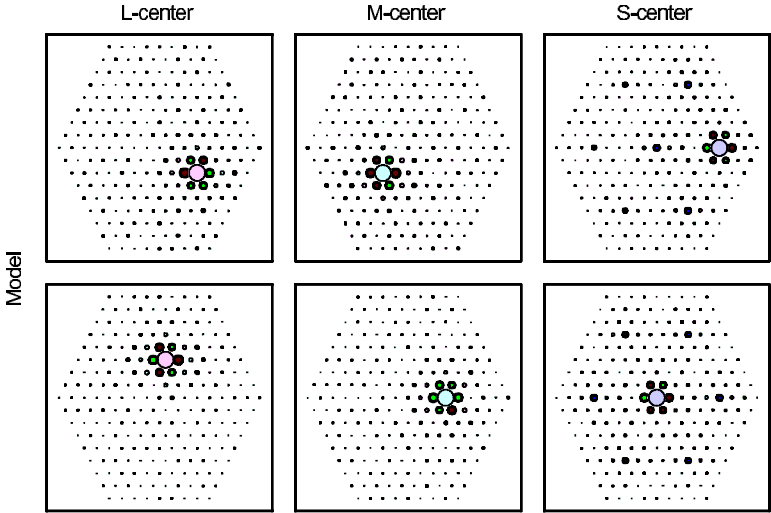
Receptive Field Organization

Figure 3: Receptive fields of the decorrelating stage. Each panel shows a weighting pattern (receptive field organization) from cone mosaic to a certain decorrelating unit. Here we show two examples for each L-, M-, and S-center type. Bright and dark circles show positive and negative weights; red, green, and blue colors correspond to weights of L-, M-, and S-cone; and the circle size indicates the amplitude of the weight.

cone type, leading to three types of units that we refer to as L-center, M-center, and S-center. All units were classified as color selective unit using the criterion in Hanazawa, Komatsu, and Murakami (2000): the Color Selectivity Index (CSI) greater than 0.5 (see Figure 4b).[1] This matches the lack of luminance or achromatic units in pLGN/kLGN (Lennie & D'Zmura, 1988; Hanazawa et al., 2000). Figure 4a illustrates color selectivity profiles in comparison with those of pLGN/kLGN neurons, showing agreement between the model and the physiological data. Figure 4c is the histogram of their color tuning directions, segregated in three clusters as in the physiological data. The color tuning directions of the L-center and M-center types were almost completely opposite (-6.3 ± 13.5 and 180.8 ± 1.9, respectively). This is also confirmed in Figure 4a, where contours of the responses were aligned in the same orientation but in the reverse order. This indicates that both the L- and M-center types were responsible for the same r-g channel,

_____

[1] (Color Selectivity Index) = [(max response) − (min response)]/[max abs(response)]. In the physiological study of Hanazawa et al. (2000), the response is defined by [mean discharge ratio] − [baseline activity]. Therefore, negative values are possible.
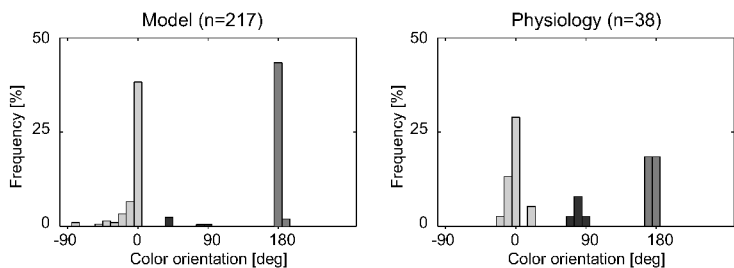
(a) Color Fields in CIExy
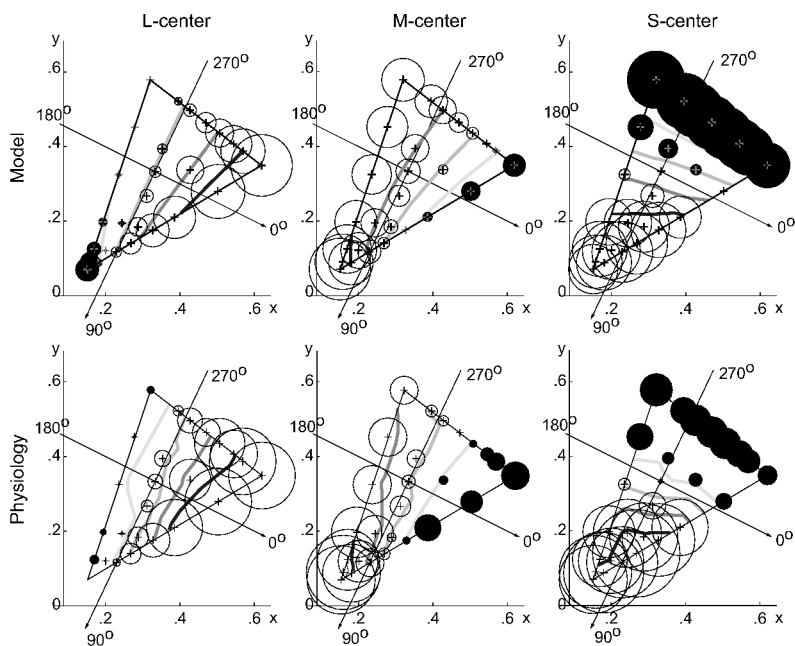
(b) Color Selectivity Index
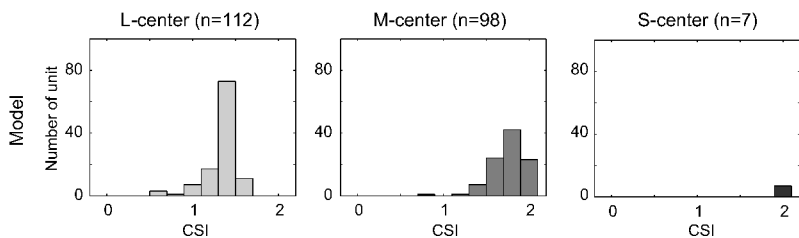
(c) Color Tuning Direction

while the S-center type was responsible for the y-b channel, in the color opponent stage.

Regarding L-center and M-center type, there was no significant cone-type specificity in the receptive field organization. In fact, they showed close similarity to the whitening filters derived from a single cone-type cone mosaic (here we used M-cone, and as a result the data are gray-scale): $\mathbf{w_Z}^T\mathbf{w_{Zgray}}/\|\mathbf{w_Z}\|\|\mathbf{w_{Zgray}}\| = 0.995 \pm 0.005$. This suggests that their receptive field organization is determined mainly by spatial factor, not by cone-type dependent chromatic factor. This also means that the significant color selectivity of L- and M-center type is mainly due to the weighting ratio between the center and the surround, itself mainly due to the spatial factor, not the cone-type specific, antagonistic wiring. These results would be reasonable since the majority of the input signals come from L- and M-cones, of which spectral sensitivities are highly overlapping. Therefore, the statistics of cone mosaic data are close to those of gray-scale (only M-cone) data.

S-center type shows S-cone specificity with larger receptive fields than L- and M-center types (see Figure 3). This is consistent with the large dendritic arborization of the small bistratified retinal ganglion cells, which are distinct from midget and parasol ganglion cells and belong to the konio-cellular (S-cone) pathway (Dacey, 2000). Our results show that the S-cone weights in the surround are inhibitory. This is reasonable since the difference of correlated signals is oriented along the uncorrelated axis. The larger size of S-center

---

Figure 4: *Facing page*. Chromatic properties of the decorrelating stage. (a) Color selectivity. Model data (upper row) were derived from the same units illustrated in the lower row of Figure 3. Physiological data (lower row) are of pLGN/kLGN neurons. This diagram shows the responses of a certain unit to a set of color stimuli distributed in both MacLeod-Boynton (MB) and CIE 1931 xy (CIE-xy) chromaticity coordinates. For illustration purposes, a CIE-xy chromaticity diagram was used. Open and filled circles show positive and negative responses, respectively; their diameters indicate response amplitudes; + corresponds to the chromaticity of the color stimuli. It is important to note that all color stimuli were adjusted to have the same luminance (isoluminant stimuli), and thus any difference among the responses of a certain unit can be attributed to its color selectivity. Contours of the responses are also plotted: from thick to thin, 80%, 60%, 40%, and 20% of [maximum response] − [minimum response]. Axes of color orientations defined in MB chromaticity coordinates are shown as well (0, 90, 180, 270 degrees). For the analysis of second-layer units, the stimuli were a uniform pattern to mimic diffuse light in the physiological experiment. (b) Distribution of color selectivity index. (c) Distribution of color tuning directions. This direction is defined by the maximum slope of the responses. Physiological data are of pLGN/kLGN. Color of the histogram is identical to that of *b*. All physiological data are from Hanazawa, Komatsu, and Murakami (2000).

type receptive fields should be due to the sparse arrangement of S-cone in the cone mosaic, since in the case of L- and M-center type, the cones next to the center respond in a highly correlated way to the center cone. While the S-cone antagonism between the center and the surround is reasonable from the redundancy reduction point of view, physiological studies showed only the spatially coextensive yellow-blue cells in retinal ganglion cells (Dacey, 2000).

3.2 ICA Stage. In the ICA stage, two main types of receptive fields emerged (see Figures 5 and 6): the majority (94.9%) of luminance type (achromatic, color nonselective) and the others (4.6%) of color-selective type. Note that this analysis was based on $\mathbf{W}$, not $\mathbf{W_I}$.

The luminance unit was similar to those derived using gray-scale samples, showing simple-cell-like receptive field with high spatial-frequency selectivity (see Figure 5a; Bell & Sejnowski, 1997; van Hateren & van der Schaaf, 1998). This suggests that the luminance units would represent spatial information (without color). Responses to isoluminant color stimuli are almost constant (see Figure 6a), and the color selectivity index was less than 0.5 for almost all luminance units (0.28 ± 0.14; see Figure 6b), showing low color selectivity. The low value of this index means that the spectral selectivity was almost identical to the luminosity function V_λ,[2] consistent with physiological data from simple cells in V1 (Lennie & D'Zmura, 1988; Lennie, Krauskopf, & Sclar, 1990).

The color-selective units were characterized by cone-type specific antagonistic regions in their receptive field, and classified into two subtypes: Y/B type of yellow-blue selectivity and R/G type of red-green selectivity. The


Figure 5: *Facing page.* Receptive fields of the ICA stage. (a) Receptive field organization. Here, each panel shows a weighting pattern from cone mosaic to a certain ICA unit. Two examples for each luminance, Y/B, and R/G type are shown. The optimal bar stimulus for the units is shown just below each receptive field. The optimal bar is defined by the bar that maximally matches the weighting pattern. A set of bars was prepared with 13 width, $1 \sim 3$ length, and 22 orientation for arbitrary location. To find the color-opponent region for color-selective type, weighting patterns were modified as follows: $+L + M - S$ for Y/B type; $+L - M$ for R/G type (S-cone is neglected). (b) Basis function. These are the dual vectors of filters shown in *a*.

---

[2] Due to the use of isoluminant color stimuli, the responses of luminosity function to the color stimuli are identical. The reverse is also true: any spectral sensitivity is written as the sum of luminosity function and its residual, $S(\lambda) = aV_\lambda(\lambda) + \Delta(\lambda)$, and the response to an isoluminant stimulus $i(\lambda)$ is $\int S(\lambda)i(\lambda)d\lambda = a\int V_\lambda(\lambda)i(\lambda)d\lambda + \int \Delta(\lambda)i(\lambda)d\lambda$, where $a \equiv \int S(\lambda)i(\lambda)d\lambda / \int V_\lambda(\lambda)i(\lambda)d\lambda$ and $a\int V_\lambda(\lambda)d\lambda$ is constant by definition. If the left side is constant over any isoluminant color stimuli, $\Delta(\lambda) = 0$; thus, $S(\lambda) = aV_\lambda(\lambda)$.
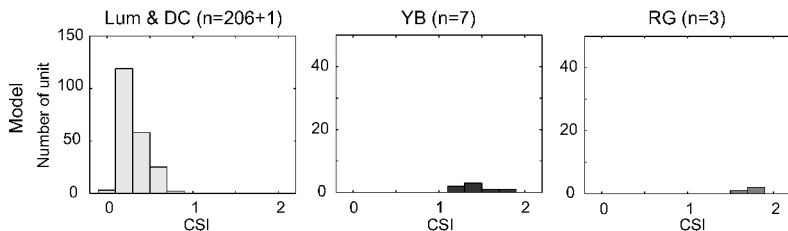
(a) Receptive Field Organization
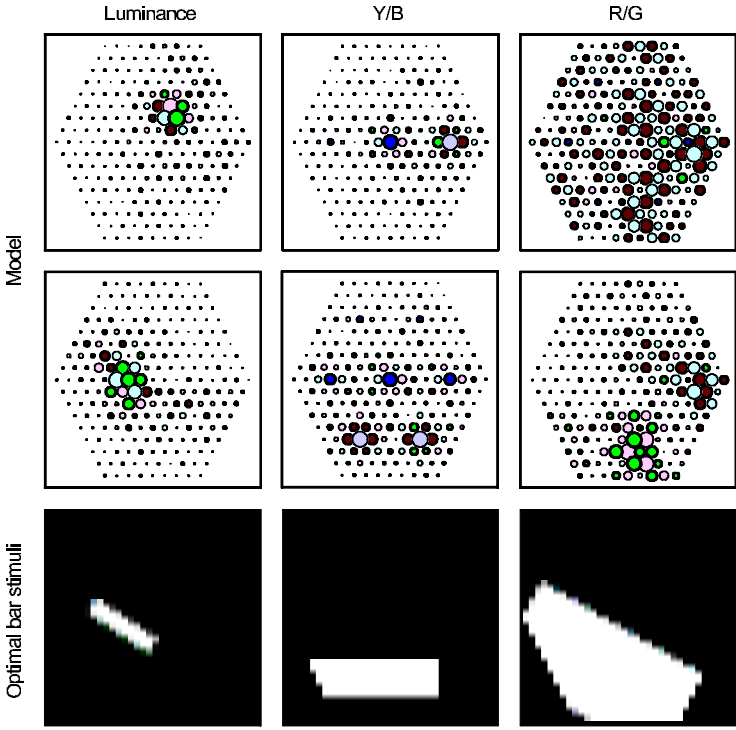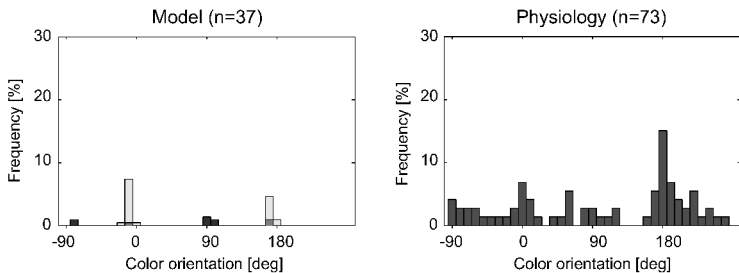

(b) Basis functions
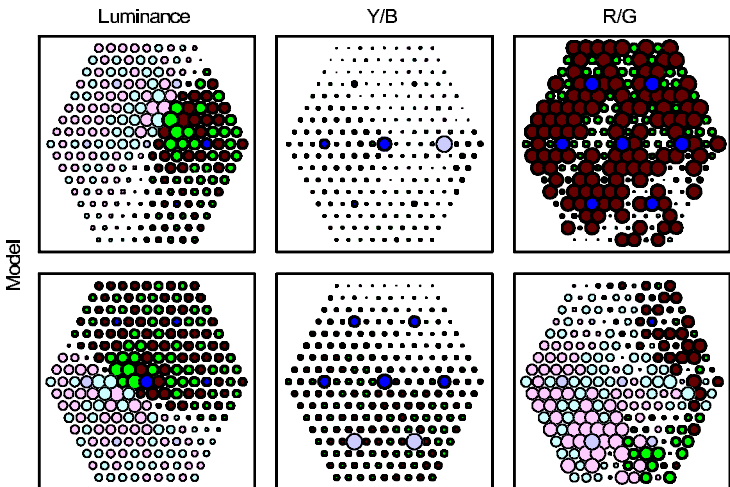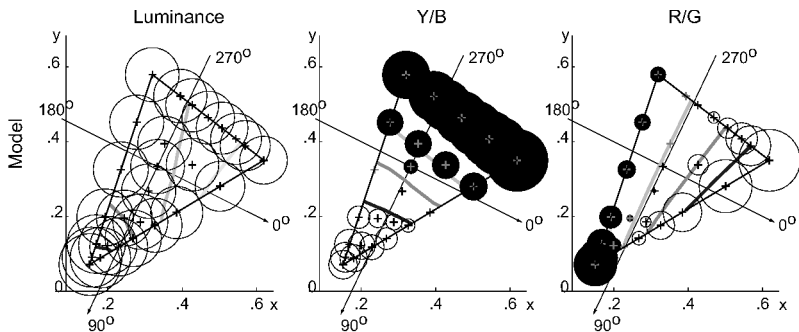
Figure 6: Chromatic properties of the ICA stage. (a) Color selectivity, derived from the units shown in the middle row of Figure 5a. For physiological data, see Figure 3A in Hanazawa et al. (2000) for R/G type; data corresponding to luminance or Y/B unit are not illustrated there, although they were reported. (b) Distribution of color selectivity index. (c) Distribution of color tuning direction. Here, those units of which CSI is greater than 0.5 are included in the analysis in accordance with the physiological study. Color of the histogram is identical to that of *b*. All physiological data are taken from Hanazawa et al. (2000).

color selectivity index was much larger than 0.5 (larger than 1) for all color-selective units (1.43 ± 0.16 for Y/B, 1.70 ± 0.01 for R/G; see also Figure 6b), indicating that they are highly color selective. Note that CSI > 1 indicates the existence of color opponency, which yields positive response to one color and negative response to another. These color-selective subtypes may correspond to the two color channels suggested in psychophysical studies (Lennie & D'Zmura, 1988). However, it does not match the physiological studies that showed distributed tuning over the color axis (see the right panel in Figure 6c; see also Figure 2 in De Valois, Cottaris, Elfar, Mahon, & Wilson, 2000). Most color-selective units showed orientation selectivity. Although the orientation selectivity of color-selective cells in V1 is controversial (Michael, 1978; Lennie et al., 1990; Conway, 2001; Johnson, Hawken, & Shapley, 2001), our results suggest that they may be expected in redundancy reduction of cone mosaic responses.

In addition to luminance units and color-selective units, we obtained a basis function showing a uniform pattern over the cone mosaic, referred to as the DC unit. Its receptive field organization was affected by the boundary effect. In a previous study, this component was excluded from the analysis by subtracting the average for each image patch (Hoyer & Hyvarinen, 2000).

Color-selective units had a larger receptive field compared to luminance units: the size of the optimal bar is 4.42 ± 3.41 (cone size) for luminance units and 36.30 ± 6.73 and 74.62 ± 25.52 for Y/B and R/G units. This is consistent with the low spatial-frequency selectivity of the color mechanism (Mullen, 1985), as expected, since the color information is derived from the comparison between at least two or three types of cones, but there is only a single cone at each retinal location. Thus, chromatic information requires averaging over several cones, leading to lower spatial-frequency selectivity. Note also that the percentage of the color-selective units was significantly lower than that of luminance units, indicating that the dimensionality assigned for chromatic information is much less than that for luminance information.

Our analysis thus far of properties of receptive fields $\mathbf{w_i}$ suggests that ICA yields two types of units: luminance units responsible for encoding spatial information without color and color-selective units responsible for color information without fine spatial information. We can rewrite the data-generative model of the cone mosaic responses (see equation 2.2) as

$$\mathbf{x} = \sum_{i \in \text{Form}} u_i \mathbf{a_i} + \sum_{j \in \text{Color}} u_j \mathbf{a_j}, \tag{3.1}$$

where we assumed that Form consists of luminance and DC units and Color consists of color-selective units. Recall that the response u_i represents the presence of the basis function $\mathbf{a_i}$ in the input $\mathbf{x}$. Some examples of the basis function are shown in Figure 5b. Regarding luminance units, the basis functions show cone-type irrespective edge pattern, exactly as the case of grayscale images. Note that even the locations of S-cone are filled in as if they

were part of the edge surface, while S-cone scarcely contributes their receptive field organization. Regarding color-selective units, the basis functions show cone-type specific patterns, that is, color information. These suggest that the statistically independent patterns in the cone mosaic responses are a large number of cone-type unspecific edge patterns and a small number of cone-type specific edge patterns, along with a spatially uniform pattern for each type. In Figure 7, we visualize these different types of information by separate images (Color is divided into R/G and Y/B for convenience). It is clear that the form information is extracted by luminance and DC units (see Figure 7c), and color information is extracted by Y/B (see Figure 7d) and R/G units (see Figure 7e) from the cone mosaic responses (see Figure 7b).

In this study, all resulting independent components had supergaussian distributions. When histogram equalization was used as a model for cone nonlinearity instead of the physiological model (see the appendix), one subgaussian component emerged whose basis function showed a DC component. This is consistent with other studies using gray-scale images (van Hateren & van der Schaaf, 1998) or LMS images (Wachtler et al., 2001), both of which applied the logarithm function as the cone nonlinearity.

3.3 PCA Comparison. The cone mosaic responses were also analyzed by principal component analysis (PCA) to compare the results with those derived from ICA. As shown in Figure 8, PCA yielded nonlocal filters as in the case of gray-scale images (Olshausen & Field, 1996; Bell & Sejnowski, 1997). There were only two components that showed cone-type specificity; both showed S-cone specificity. This means that the spatial variation (variance)

Figure 7: *Facing page*. Illustration of information content in Luminance, Y/B, or R/G channel. (a) RGB image. (b) Cone mosaic responses. This is the same as Figure 1e but for another natural scene. (c) Reconstruction from luminance and DC units. For each small patch of cone mosaic frame, the image $\hat{\mathbf{x}}$ was reconstructed by $\hat{\mathbf{x}} = \sum_i u_i \mathbf{a_i}$, where i indicates luminance and DC units. These patches were tiled over the whole image. (d) Reconstruction from Y/B units. As in c above, but i indicates Y/B units. We also postprocessed the image to represent it using pseudocolor: L- and M-cones are regarded as contributing yellow direction (i.e., R- and G-pixels with like sign; B-pixel with opposite sign); S-cone is regarded as blue direction (B-pixel with like sign; R- and G-pixels with opposite sign). To avoid dark pixels, with color hard to see, the base color is set to be gray. (e) Reconstruction from R/G units. As in d, except that i indicates R/G units. In postprocessing, L- and S-cones are regarded as contributing red direction (i.e., R-pixel with like sign, G-pixel with opposite sign); M-cone is regarded as green direction (G-pixel with like sign; R-pixel with opposite sign). Any B-pixel is set as 0. As in d, the base color is set gray. (f) Superimposing luminance, R/G, and Y/B information above to see form and color information simultaneously.
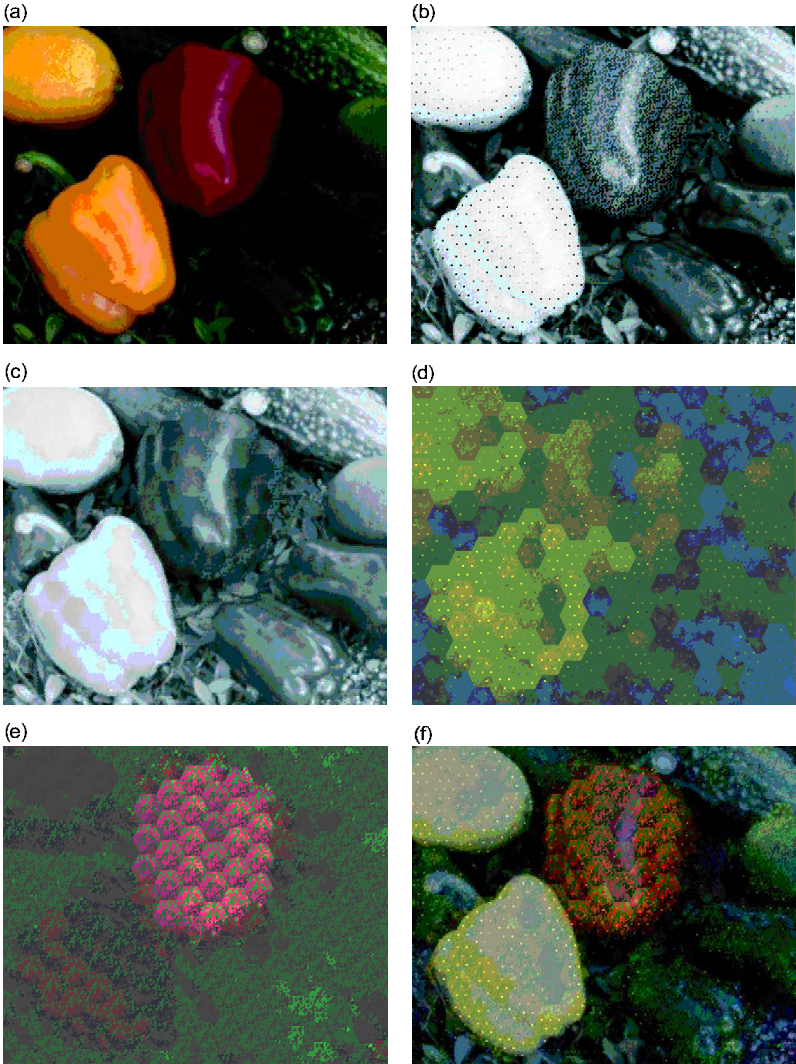
common with all cone-type dominates the chromatic variation specific for each cone type (especially for L- and M-cone type). When LMS natural images are analyzed by PCA, Y/B and R/G components were as common as black-white components (Ruderman, Cronin, & Chiao, 1998). This demonstrates that it is not straightforward for the visual system to extract color information from the cone mosaic responses.
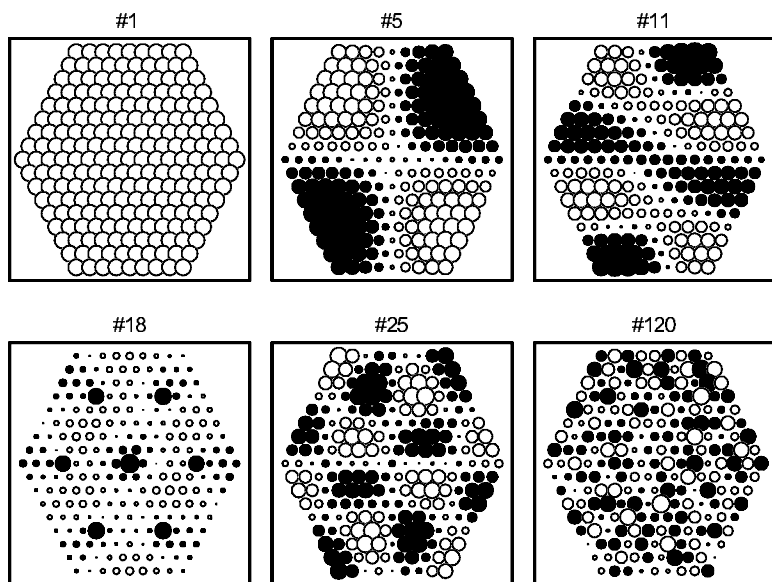
Figure 8: Principal components of cone mosaic responses. Here we show the 1st, 5th, 11th, 18th, 25th, and 120th principal component, as indicated for each panel. Here, cone type is not indicated by color, but otherwise these are the same illustrations as Figures 3 and 5a. Cone-type specificity can be seen in only two units that show S-cone specificity; the eighteenth component is one of them. The first component is exactly the same as the DC type basis function in the ICA stage.

4 Discussion

4.1 Multiplexing and Separating Stages. It has been suggested that in the pLGN/kLGN, luminance information is conveyed with red-green information in the r-g opponent channel and that these "multiplexed" signals are "separated" into red-green and luminance information in the following stages, possibly in V1 (Ingling & Martinez-Uriegas, 1983; Lennie & D'Zmura, 1988; Lennie et al., 1990). Our results reproduce this two-stage model. We emphasize that this is an emergent property derived from redundancy reduction and not put in by hand as in the previous model studies (Billock, 1991; De Valois & De Valois, 1993; Kingdom & Mullen, 1995). These results suggest mechanisms by which the visual system could reduce redundancy in a sequence of stages.

4.2 Learning Visual Information Processing. It is possible that the color selectivity properties of neurons in the visual system are the end result of

evolution, and during development they are implemented without visual experience. All of the properties of the cells in our model were obtained with unsupervised algorithms. This suggests that some of the properties of cells in both pLGN/kLGN and V1 could be acquired by unsupervised learning during development from visual input. Other properties of cortical neurons, such as orientation and direction selectivity, depend on the visual experience during development (Blakemore & Cooper, 1970; Blakemore & van Sluyters, 1975). Studies of natural scene statistics also support this idea (Olshausen & Field, 1996; Bell & Sejnowski, 1997; van Hateren & van der Schaaf, 1998). There are several psychophysical studies investigating the plasticity of color vision during development (Teller, 1998; Knoblauch, Vital-Durand, & Barbur, 2001); however, the physical basis of plasticity in color vision has not yet been examined. Our results suggest that color selectivity, like orientation selectivity, may depend on the statistics of sensory signals. They also suggest that in general, the visual coding of attributes such as form and color (Livingstone & Hubel, 1988) can be understood as a result of redundancy reduction.

4.3 Relation to Previous Studies. Other studies applying ICA to RGB images (Tailor et al., 2000; Hoyer & Hyvarinen, 2000) used spectral sensitivities unlike those found in the human retina, which precludes direct comparisons to physiological or psychophysical data. We used spectral sensitivities of human cone photoreceptors, enabling us to obtain results under more realistic conditions. A similar approach was used earlier (Wachtler et al., 2001; Lee, Wachtler, & Sejnowski, 2002), but without sampling of a trichromatic cone mosaic. We examined the additional constraint that spatial separability of chromatic signals imposes on the human visual system and found that in contrast with the results of previous studies, (1) the cone-type specificities for color vision can be learned under the realistic and difficult condition due to the cone mosaic sampling; (2) the spectral sensitivity of simple-cell-like units is along the luminance axis, not the black-white axis; (3) the percentage of luminance (simple-cell like) units is large (>90%), not low (about 1/3); and (4) the luminance units show higher spatial-frequency selectivity than color-selective units.

5 Conclusion

The goal of this study was to analyze the cone mosaic responses to natural scenes and to find an efficient coding of spatiochromatic signals in the visual system. Our results suggest that a hierarchical redundancy reduction model explains the spatiochromatic properties of neurons in the early stages of processing in the visual system.

Although our model used more realistic inputs than previous approaches (Tailor, et al., 2000; Hoyer & Hyvarinen, 2000; Wachtler et al., 2001), it still assumes a linear transformation. Thus, the current model cannot capture

complex properties such as nonlinear combination of cone signals (De Valois et al., 2000) or contextual interactions (Wachtler, Sejnowski, & Albright, 1999). Our model nevertheless approximates the early processing stages of the visual system. The similarities between our results and the known properties of the visual system further strengthen the hypothesis that redundancy reduction is an organizing principle in the visual system.

Appendix: Preparation of Cone Responses to Natural Scenes

Images of 62 natural scenes was obtained using 3CCD digital still camera system (HC-2500, Fujifilm, Japan). Each RGB image (1000 × 1280 pixels, 10 bits for each R, G, B) were corrected for gamma calibration, effect of iris size, and exposure time. These linear RGB data, of which spectral sensitivities were also measured, were transformed into LMS cone responses using a 3×3 matrix. This matrix was derived by minimizing square errors for 170 surface reflectance functions (Vrhel, Gershon, & Iwan, 1994) rendered by four kinds of CIE daylight functions (D50, D55, D65, and D75). The resulting errors were 0.23%, 0.14%, and 0.04% for L-, M-, and S-cone, respectively. Its approximation accuracy was also evaluated by a different set of reflectance functions (ColorCheker, Macbeth, U.S.A.), and the estimation errors were reasonably small as 0.39%, 0.23%, and 0.03% for L-, M-, and S-cone, respectively. These linear cone response data were further transformed with an empirical cone nonlinear function (Baylor, Nunn, & Schnapf, 1987) given by

$$r_{nl} = 1 - \exp(-k \cdot r_l), \tag{A.1}$$

where r_l is linear cone responses, r_{nl} is nonlinearly transformed cone responses, the range of which is [0,1], and the parameter k is determined so that the median of r_l is 0.5 for each scene and for each cone type. We did not apply any preprocessing of the data such as low-pass filtering (Olshausen & Field, 1996) or dimensionality reduction using PCA (van Hateren & van der Schaaf, 1998).

Acknowledgments

References

Amari, S., Cichocki, A., & Yang, H. (1996). A new learning algorithm for blind signal separation. In D. Touretzky, M. Mozer, & M. Hasselmo (Eds.), *Advances in neural information processing systems, 8*, (pp. 757–763). Cambridge, MA: MIT Press.

Atick, J. J. (1992). Could information theory provide an ecological theory of sensory processing? *Network, 3*, 213–251.

Atick, J. J., & Redlich, A. N. (1993). Convergent algorithm for sensory receptive field development. *Neural Computation, 5*, 45–60.

Barlow, H. B. (1961). Possible principles underlying the transformation of sensory messages. In W. A. Rosenblith (Ed.), *Sensory communication* (pp. 217–234). Cambridge, MA: MIT Press.

Baylor, D. A., Nunn, B. J., & Schnapf, J. L. (1987). Spectral sensitivity of cones of the monkey macaca fascicularis. *Journal of Physiology, 390*, 145–160.

Bell, A. J., & Sejnowski, T. J. (1995). An information-maximization approach to blind separation and blind deconvolution. *Neural Computation, 7*, 1129–1159.

Bell, A. J., & Sejnowski, T. J. (1997). The independent components of natural scenes are edge filters. *Vision Research, 37*, 3327–3338.

Billock, V. A. (1991). The relationship between simple and double-opponent cells. *Vision Research, 31*, 33–42.

Blakemore, C., & Cooper, G. F. (1970). Development of the brain depends on the visual environment. *Nature, 228*, 477–478.

Blakemore, C., & van Sluyters, R. C. (1975). Innate and environmental factors in the development of the kitten's visual cortex. *Journal of Physiology, 248*, 663–716.

Cardoso, J. F. (1997). Infomax and maximum likelihood for source separation. *IEEE letters on Signal Processing, 4*, 112–114.

Conway, B. R. (2001). Spatial structure of cone inputs to color cells in alert macaque primary visual cortex (v-1). *Journal of Neuroscience, 21*, 2768–2783.

Dacey, D. M. (2000). Parallel pathways for spectral coding in primate retina. *Annual Review of Neuroscience, 23*, 743–775.

de Monasterio, F. M., McCrane, E. P., Newlander, J. K., & Schein, S. J. (1985). Density profile of blue-sensitive cones along the horizontal meridian of macaque retina. *Investigative Ophthalmology and Visual Science, 26*, 289–302.

De Valois, R. L., Cottaris, N. P., Elfar, S. D., Mahon, L. E., & Wilson, J. A. (2000). Some transformations of color information from lateral geniculate nucleus to striate cortex. *PNAS, 97*, 4997–5002.

De Valois, R. L., & De Valois, K. K. (1993). A multi-stage color model. *Vision Research, 33*, 1053–1065.

Field, D. J. (1994). What is the goal of sensory coding? *Neural Computation, 6*, 559–601.

Girolami, M. (1999). *Self-organizing neural networks: Independent component analysis and blind source separation.* New York: Springer-Verlag.

Golub, G. H., & Loan, C. F. (1996). *Matrix computation* (3rd ed.). Baltimore: Johns Hopkins University Press.

Hanazawa, A., Komatsu, H., & Murakami, I. (2000). Neural selectivity for hue and saturation of colour in the primary visual cortex of the monkey. *European Journal of Neuroscience, 12*, 1753–1763.

Hoyer, P. O., & Hyvarinen, A. (2000). Independent component analysis applied to feature extraction from color and stereo images. *Network, 11*, 191–210.

Hyvarinen, A., Karhunen, J., & Oja, E. (2001). *Independent component analysis*. New York: Wiley.

Ingling, C. R. Jr., & Martinez-Uriegas, E. (1983). The relationship between spectral sensitivity and spatial sensitivity for the primate r-g X-channel. *Vision Research, 23*, 1495–1500.

Johnson, E. N., Hawken, M. J., & Shapley, R. (2001). The spatial transformation of color in the primary visual cortex of the macaque monkey. *Nature Neuroscience, 4*, 409–416.

Kingdom, F. A. A., & Mullen, K. T. (1995). Separating colour and luminance information in the visual system. *Spatial Vision, 9*, 191–219.

Knoblauch, K., Vital-Durand, F., & Barbur, J. L. (2001). Variation of chromatic sensitivity across the life span. *Vision Research, 41*, 23–36.

Lee, T.-W. (1998). *Independent component analysis: Theory and applications*. Norwell, MA: Kluwer.

Lee, T.-W., Girolami, M., & Sejnowski, T. J. (1999). Independent component analysis using an extended infomax algorithm for mixed subgaussian and supergaussian sources. *Neural Computation, 11*, 417–441.

Lee, T.-W., Wachtler, T., & Sejnowski, T. J. (2002). Color opponency is an efficient representation of spectral properties in natural scenes. *Vision Research, 42*, 2095-2103.

Lennie, P., & D'Zmura, M. (1988). Mechanisms of color vision. *CRC Critical Reviews on Neurobiology, 3*, 333–400.

Lennie, P., Krauskopf, J., & Sclar, G. (1990). Chromatic mechanisms in striate cortex of macaque. *Journal of Neuroscience, 10*, 649–669.

Livingstone, M., & Hubel, D. (1988). Segregation of form, color, movement, and depth: Anatomy, physiology, and perception. *Science, 240*, 740–749.

Michael, C. R. (1978). Color vision mechanisms in monkey striate cortex: Simple cells with dual opponent-color receptive fields. *Journal of Neurophysiology, 41*, 1233–1249.

Mollon, J. D., & Bowmaker, J. K. (1992). The spatial arrangement of cones in the primate fovea. *Nature, 360*, 677–679.

Mullen, K. T. (1985). The contrast sensitivity of human color vision to red-green and blue-yellow chromatic gratings. *Journal of Physiology, 359*, 381–400.

Olshausen, B. A., & Field, D. J. (1996). Emergence of simple-cell receptive field properties by learning a sparse code for natural images. *Nature, 381*, 607–609.

Ruderman, D. L., Cronin, T. W., & Chiao, C.-C. (1998). Statistics of cone responses to natural images: Implications for visual coding. *Journal of the Optical Society of America A, 15*, 2036–2045.

Stockman, A., & Sharpe, L. T. (2000). Spectral sensitivities of the middle- and long-wavelength sensitive cone derived from measurements in observers of known genotype. *Vision Research, 40*, 1711–1737.

Szel, A., Diamantstein, T., & Rohlich, P. (1988). Identification of the blue-sensitive cones in the mammalian retina by anti-visual pigment antibody. *Journal of Comparative Neurology, 273*, 593–602.

Tailor, D. R., Finkel, L. H., & Buchsbaum, G. (2000). Color-opponent receptive fields derived from independent component analysis of natural images. *Vision Research, 40*, 2671–2676.

Teller, D. Y. (1998). Spatial and temporal aspects of infant color vision. *Vision Research, 38*, 3275–3282.

van Hateren, J. H., & van der Schaaf, A. (1998). Independent component filters of natural images compared with simple cells in primary visual cortex. *Proceedings of Royal Society of London B, 265*, 359–366.

Vrhel, M. J., Gershon, R., & Iwan, L. S. (1994). Measurement and analysis of object reflectance spectra. *Color Research and Application, 19*, 4–19.

Wachtler, T., Lee, T.-W., & Sejnowski, T. J. (2001). Chromatic structure of natural scenes. *Journal of Optical Society of America A, 18*, 65–77.

Wachtler, T., Sejnowski, T. J., & Albright, T. D. (1999). Interactions between stimulus and background chromaticities in macaque primary visual cortex. *Investigative Ophthalmology and Visual Science, 40*, 641.